A Applied

S. Šturm et al.: The role of Si impurities in the transient dopant segregation and precipitation in yttrium-doped alumina

Sašo Šturm[a], Mehmet A. Gülgün[b], Gunther Richter[c], Francisco M. Morales[d], Rowland M. Cannon[e], Manfred Rühle[c]

[a] Jožef Stefan Institute, Department for Nanostructured Materials, Ljubljana, Slovenia
[b] Sabanci University, FENS, Tuzla, Istanbul, Turkey
[c] Max-Planck-Institute für Metallforschung, Stuttgart, Germany
[d] Universidad de Cadiz, Puerto Real, Spain
[e] MSD, Lawrence Berkeley National Laboratory, Berkeley, U.S.A.

The role of Si impurities in the transient dopant segregation and precipitation in yttrium-doped alumina

Y-doped alumina was sintered at 1500 °C for 10 h under ultra-clean experimental conditions without experiencing any abnormal grain growth. The yttrium was fairly homogeneously distributed at the grain boundaries, with a mean value of $\overline{\Gamma}_Y = 5.5$ at nm^{-2}. The Y–Al–O precipitates in the clean, Y_2O_3-doped alumina specimen were the YAP ($YAlO_3$) phase, whereas only the YAG ($Y_3Al_5O_{12}$) phase was present in the Y_2O_3-doped alumina samples contaminated with SiO_2. The excess concentrations of Y and Si atoms at the grain boundaries that, at the same time, provoke the formation of structurally complex YAG precipitates and abnormal grain growth were both estimated to be at $4-5$ at nm^{-2}. The compositions of the triple point pocket phases found in the region of the exaggeratedly grown alumina grains indicate the presence of alumino-silicate bulk liquids at the sintering temperature.

Keywords: Precipitation; Grain boundary segregation; Interfaces; Abnormal grain growth; Electron energy loss spectroscopy (EELS)

1. Introduction

Several investigations have shown that in high-purity alumina doped with Y_2O_3 the initial yttrium grain-boundary excess concentration increase monotonically to the point where the grain boundaries are saturated with a critical amount of yttrium [1–8]. Above this level Y–Al–O precipitates form and the excess concentration of yttrium at the grain boundaries levels off at a constant value. A further increase in the amount of yttrium dopants only results in an increased volume of precipitates.

The binary phase diagram between Al_2O_3 and Y_2O_3 predicts that precipitation in the "supersaturated" yttrium-doped alumina proceeds via the formation of the aluminium-richest phase, yttrium aluminate garnet, YAG ($Y_3Al_5O_{12}$) [9, 10]. Conversely, recent studies have shown that the first yttrium aluminate precipitate is yttrium aluminate perovskite phase, YAP ($YAlO_3$), and this can coexist in the presence of YAG and α-Al_2O_3 [8]. This apparent contradiction with the Gibbs phase rule was attributed to the kinetic constraints at the grain boundaries that promote the formation of the structurally simple YAP phase (20 atoms/unit cell), rather than nucleating the YAG phase, containing 160 atoms/unit cell.

In Al_2O_3 with only Y_2O_3 [5], the microstructure of the ceramic consisted of equiaxed, fine-grained alumina grains. However, the Y_2O_3-doped alumina ceramic when intentionally infested with an Si impurity, experienced abnormal grain growth (AGG) [1, 11]. The role of the SiO_2 in yttrium-doped alumina on the grain-boundary mobility was, to a certain extent, revealed by MacLaren et al. [12]. They showed that under specified sintering conditions SiO_2 alone would not promote AGG, while it was regularly observed in the presence of SiO_2 and Y_2O_3. Different grain-boundary mobilities in the Si–Y-doped alumina system were related to the disordered grain-boundary core structure and the subsequent development of an intergranular film that is $1-2$ nm thick [12–14]. Several generalized mechanisms for rapid grain-boundary motion suggest that dopants can interact with each other and the host ions in order to change the grain-boundary structure and/or the diffusivities, which have an effect on the mobility of the grain boundaries or pores [14–18].

From studies that have been performed in Y_2O_3-doped alumina systems with a low concentration of Si impurities it is not clear whether the formation of metastable intergranular phases such as grain-boundary films, precipitates and triple-point pocket phases are related to the phases in the $SiO_2-Y_2O_3-Al_2O_3$ equilibrium ternary phase diagram [19, 20]. To clarify the formation of phases and different microstructures when moving from the pure to the Si-contaminated Y_2O_3-doped alumina system, the role of Si impurities was mainly associated with the following questions:

- How do the Si impurities affect the dopant segregation and the formation of Y–Al–O precipitates in yttrium-doped alumina?
- Is the micro-chemistry of Si-contaminated yttria-doped alumina related to the existing phases in the Y–Al–Si equilibrium ternary phase diagram?

For that reason, both clean and Si-contaminated yttrium-doped polycrystalline alumina were systematically studied. A detailed structural and compositional analysis of the precipitates, the triple-point pockets and the grain-boundaries' excess concentration of Si and Y was performed.

A Applied

S. Šturm et al.: The role of Si impurities in the transient dopant segregation and precipitation in yttrium-doped alumina
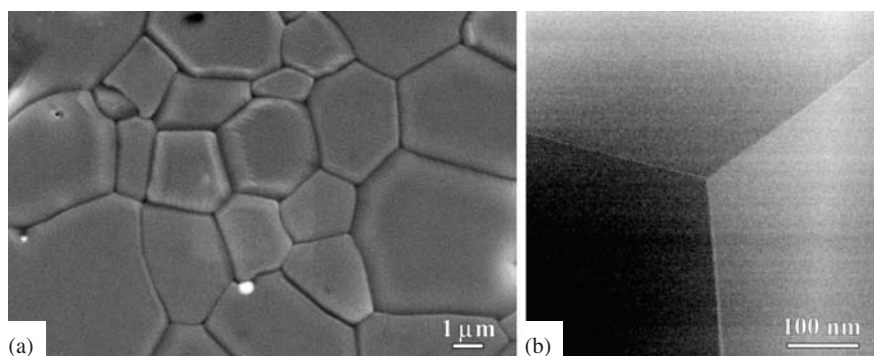
Fig. 1. (a) Clean, yttrium-doped alumina: SEM micrograph of the characteristic microstructure of yttrium-doped alumina revealing dense, fine-grained equiaxed alumina grains. The bright phase located at the grain boundaries is due to the formation of the Y–Al–O precipitate phase. (b) HAADF-STEM image showing three neighbouring alumina grains. The bright contrast at the grain boundaries is due to the segregation of Y atoms.

2. Experimental procedures

Powders were prepared from high-purity (99.995 %) α-Al_2O_3 (AKP-3000 Sumitomo Chemical Co., Osaka, Japan) with the addition of 2000 wt.ppm of Y_2O_3 (ACS-grade high-purity $Y(NO_3)_3 \cdot 6H_2O$, Strem Chemicals, Newburyport, MA, U.S.A.). The bulk concentrations of the Y_2O_3 dopant and the other impurities in these powder samples were determined using the ICP-OES technique. The results confirmed the expected doping levels of Y_2O_3 and showed no significant impurity levels [2, 3, 5].

Two different specimen-preparation routines were used. Green bodies formed from powder specimens were shaped, either in Si-based polymer moulds or an Si-free natural latex mould, by cold isostatic pressing at 800 MPa. The green bodies were then sintered in an ultra-pure single-crystal sapphire tube furnace to prevent any contamination of the specimens from the $MoSi_2$ heating elements [21]. To reduce the SiO_2 contamination further, the single-crystal sapphire tube was washed in concentrated HF acid before each sintering experiment and heated up to 1300 °C in a reducing atmosphere for several hours. The sintering was at 1500 °C for 10 h using a predefined heating schedule with a constant flow of oxygen (99.999 % purity) [22]. The samples were cooled down at 30 K min^{-1}.

High-resolution transmission electron microcopy (HRTEM) of triple point pocket phases was performed in a JEOL JEM ARM 1250 with an acceleration voltage of 1250 keV and a point-to-point resolution of 0.12 nm. Segregation levels at the grain boundaries as well as the compositional variations at the triple pockets and the precipitates were determined with a dedicated scanning transmission electron microscope (STEM) VG Microscopes HB-501 UX fitted with a cold field-emission gun and equipped with a Gatan Enfina 776 electron energy-loss spectrometer (EELS) and an ultra-thin window Si(Li) energy-dispersive X-ray spectroscope (EDXS) detector (Noran, Voyager, Middleton, WI). The precipitates in the microstructure were identified by determining the phase-specific electron energy-loss near-edge structures (ELNES) [8]. The excess concentration of segregates was measured using the "box method", as proposed by Ikeda et al. [23], and optimized for measurements of the segregated atoms at the alumina grain boundaries [24, 25]. The cation ratio was determined from the X-ray intensity ratios using the experimental Cliff–Lorimer factors [26]. The detection limit for Y was 0.28 at nm^{-2}, whereas for Si and Ca the limits were 0.25 at nm^{-2} and 0.23 at nm^{-2}, respectively. The final excess concentration of segregates was corrected for the effects of X-ray absorption and beam broadening in the alumina foil.

3. Results

In the results section a detailed structural and compositional analysis of the grain boundaries, the precipitates and the triple-point pockets is presented for:
1. yttrium-doped alumina samples with no detected Si impurities (clean yttrium-doped alumina),
2. Si-contaminated yttrium-doped alumina samples (Si-contaminated yttrium-doped alumina).

3.1. Clean yttrium-doped alumina

Figure 1a shows the microstructure of a clean, Y_2O_3-doped alumina ceramic. The microstructure reveals a dense ceramic with fine-grained equiaxed alumina grains. The particles with a bright contrast are Y–Al–O precipitates. The microstructure was uniform throughout the whole sintered body, including the outer edges of the pellet.

EDXS and EELS analyses confirmed that the only dopant detected at the grain boundaries and the triple pockets was Y. A high-angle annular dark-filed (HAADF) STEM image of three neighbouring alumina grains is shown in Fig. 1b. The bright contrast observed at the grain boundaries is due to the segregation of the heavy Y atoms to the grain-boundary core. In Fig. 2, the values of six grain-boundary Y-excess concentrations are plotted against the total amount of dopant. This so-called Cannon-plot representation is clearer in terms of showing the distribution of
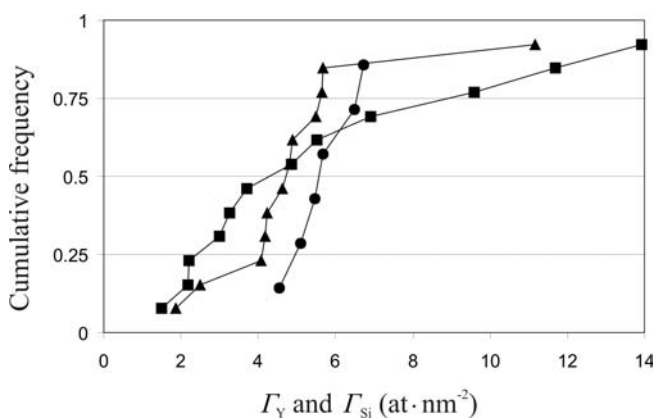

Fig. 2. Cumulative frequency chart from the measured grain-boundary chemistry for clean and Si-contaminated yttrium-doped alumina. Measurements of Γ_Y in (i) Clean, yttrium-doped alumina are marked by circles (●), whereas measurements that represent the Γ_Y and Γ_{Si} from (ii) Si-contaminated yttrium-doped alumina (region-I in Fig. 4) are shown as triangles (▲) and squares (■), respectively.

the grain-boundary chemistry and not just the average value [5]. The data points of the grain-boundary excess-Y concentration for the clean, Y_2O_3-doped alumina are marked with circles (●). The narrow distribution of the excess-Y concentration indicates a fairly homogeneous Y grain-boundary coverage. The mean excess-$\overline{Y}$ concentration of this sample, estimated from Fig. 2, was $\overline{\Gamma}_Y = 5.5$ at nm^{-2}.

Besides the grain-boundary analysis, ELNES measurements were performed on the Y–Al–O precipitates of the same specimen. The precipitates were isometric in shape, with a typical grain size smaller than 500 nm. They were found to be located both at the grain boundaries and inside the alumina grains. Background-subtracted spectra taken from the investigated precipitate are shown in Fig. 3a. It was shown previously that each standard spectrum for the Al–$L_{2,3}$ and O–K ionization edges taken from the alumina and Y-rich standards (YAP, YAG, yttrium aluminate monoclinic phase (YAM)) exhibits a unique fine structure, which makes it possible to distinguish between the different

Fig. 3. (a) Al–$L_{2,3}$ and (b) O–K ELNES of precipitate phases from clean and Si-contaminated yttrium-doped alumina samples. The fine structure of the precipitate phase from clean yttrium-doped alumina corresponds to the reference spectra taken from the standard YAP phase, whereas precipitates from the Si-contaminated yttrium-doped alumina samples correspond to the YAG phase. For reference spectra of the Y–Al–O standards see Ref. [8].

precipitate types [8]. The spectral features from the representative precipitate phase, i. e., Al–$L_{2,3}$, and the O–K spectra match perfectly with the reference spectra taken from the YAP (YAlO$_3$) and not the YAG standard (Y$_3$Al$_5$O$_{12}$), as was generally believed to be the case in low-yttrium-doped alumina specimens.

3.2. Si-contaminated yttrium-doped alumina

The samples that were pressed in Si moulds revealed a more heterogeneous microstructure. These samples were assumed to be simulating a compact whose surfaces were contaminated with Si impurities, which during sintering diffused into the interiors of the pellets. The interior of these specimen pellets was characterized by a uniform fine-grained alumina matrix. The outer rim of the pellet, presumably with the highest concentration of Si impurity, was composed of abnormally grown alumina grains with sizes up to 100 μm. Figure 4 shows the transition region between the uniform, fine-grained alumina matrix interior (region-i) and the exaggeratedly grown alumina grains at the outer rim (region-ii). The later stages of AGG, with large-sized alumina grains, are evident close to the surface of the specimen (region-ii).

Detailed EDXS analysis of the grain boundaries from the fine-grained alumina matrix (region-i in Fig. 4) revealed the co-segregation of the Y and Si atoms. Besides Y and Si no other foreign cations were detected in the specimen. The corresponding cumulative frequency distribution of Γ_Y and Γ_{Si} is shown in Fig. 2, marked by triangles (▲) and squares (■), respectively. The distribution of Γ_Y and Γ_{Si} in this case is rather wide ($1 < \Gamma_Y < 11$ and $1 < \Gamma_{Si} < 13$ at nm^{-2}). The mean excess concentrations of Y and Si atoms at all the investigated grain boundaries were $\overline{\Gamma}_Y = 4.7$ and $\overline{\Gamma}_{Si} = 4.3$ at nm^{-2}, respectively.

Small triple point (TP) pocket phases were observed in the region of the uniform fine-grained alumina matrix (region-i in Fig. 4). The typical size of the TP-pocket phases was between 10 and 50 nm. Assuming that the solid solubilities of the Si and Y atoms in the alumina matrix are negligible [27, 28], the Si/Si + Y ratio, defined as SiO$_2$/(SiO$_2$ + Y$_2$O$_3$), represents the true relative composition of the TP-pocket phases, although the neighbouring alumina grains were likely to be co-irradiated by the electron beam during the EDXS analysis of the pocket phases. Seven measurements were performed, which revealed two distinctive types of TP-pocket-phase compositions. The average composition from four measurements was 0.52 ± 0.04. This result is significantly different from the average composition
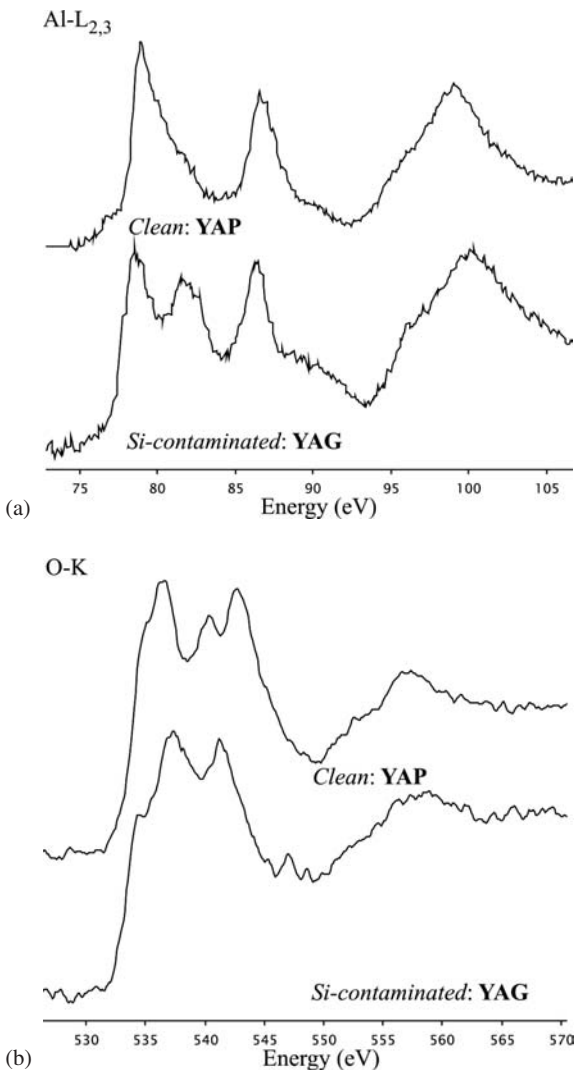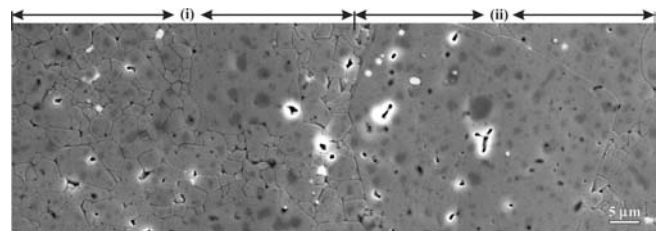
Fig. 4. Si-contaminated yttrium-doped alumina: SEM micrograph of the transition between the (i) fine-grained alumina matrix interior and the (ii) exaggeratedly grown alumina grains at the outer rim of the specimen pellet.

A Applied

S. Šturm et al.: The role of Si impurities in the transient dopant segregation and precipitation in yttrium-doped alumina

of three other measurements, which was 0.70 ± 0.01. These compositions of the TP-pocket phases were close to the composition of the crystalline Si–Y–O phases existing in the SiO_2–Y_2O_3–Al_2O_3 equilibrium ternary phase diagram, i. e., Y_2SiO_5 (Si/Si + Y = 0.5) and $Y_2Si_2O_7$ (Si/Si + Y = 0.67) [19, 20].

An examination of the region close to the surface of the specimen characterized by the exaggeratedly grown alumina grains (region-ii in Fig. 4) revealed several different types of TP-pocket phases. One type of secondary phase, occasionally observed at the grain boundaries between two adjacent, exaggeratedly grown alumina grains is shown in Fig. 5. The bright, elongated lens-like phase observed in the HAADF-STEM image is approximately 300 nm long and 40 nm wide. The EDXS results revealed that the analyzed phase is rich in Si, although a minor quantity of Y atoms was also detected (P-1 in Fig. 5). The calculated Si/Si + Y ratio was $0.85 + 0.04$. The analysis of the grain boundary, 20 nm away from the bright phase (P-2), revealed a very high concentration of Si atoms, with a Si/Si + Y ratio of 0.91 ± 0.05. The Y and Si excess concentrations from this part of the GB were
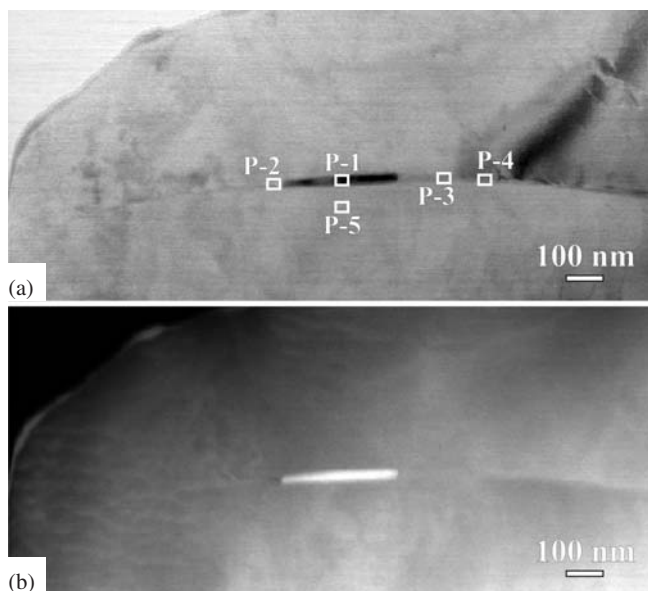

Fig. 5. (a) BF-STEM and (b) HAADF-STEM images of a lens-like phase located at the grain boundary between two exaggeratedly grown alumina grains. The EDXS results from the marked areas are summarized in the Results section.

$20.4 + 0.2$ and 97.2 ± 0.1 at nm^{-2}, respectively. However, analyses performed on the same grain boundary, approximately 100 nm away from the bright phase (P-3 and P-4), revealed average values for Γ_Y and Γ_{Si} of 3.2 ± 0.6 and 3 ± 0.8 at nm^{-2}, respectively. The measurements performed on the bulk region of the alumina grains (P-5) showed no statistically significant concentration of Y and Si atoms.

Another type of secondary phase is the well-defined homogeneous phase occupying a large portion of the TP-pocket region (Fig. 6a). The composition of this TP-pocket phase was, on average, 71 mol.% SiO_2, 25 mol.% Y_2O_3 and 4 mol.% Al_2O_3. A small quantity of the other minor phase was observed at the tip of the triple-point junctions, where the neighbouring alumina grains meet (marked with an arrow in Fig. 6a). The analysis of this minor phase revealed mainly the presence of SiO_2, with a small amount of Al_2O_3 (96 mol.% SiO_2 and 4 mol.% Al_2O_3). Similar TP-pocket structures were verified by HRTEM, as shown in Fig. 6b, where the crystallite is occupying the central pocket region, while amorphous regions are still present at the grain junctions.

The compositions of the TP-pocket phases are marked in the equilibrium Al_2O_3–SiO_2–Y_2O_3 ternary phase diagram (Fig. 7). Altogether, 42 TP-pocket phase compositions were analyzed. Measurements of the TP-pocket phases smaller than the selected analytical window were also quantified. The concentration of Al atoms in such cases was most likely overestimated, due to the possible co-irradiation of adjacent alumina grains. These measurements with an overestimated Al_2O_3 concentration are shown as squares (■), whereas the measurements that represent the correct composition of the triple-pocket phases are marked as circles (●). The grey diamond symbol (◆) represents the composition of the lowest ternary eutectic of the system at $1371 \pm 5\,°C$. These compositions are superimposed on the two isothermal sections of the reported Y_2O_3–Al_2O–SiO_2 system at $1400\,°C$ and $1600\,°C$ [19]. These two sections show the estimated extent of the liquid region in the equilibrium phase diagram. An increased density of experimental points was observed close to the $Y_2Si_2O_7$ phase. Another group of measured compositions was scattered in the broad liquid region, with a few data points close to the ternary eutectic point.

Besides Y- and Si-rich TP-phases, precipitates a few microns in size, which appear bright in the HAADF-STEM images, were also observed and analyzed. Several of these precipitates were investigated using EDXS and EELS ana-
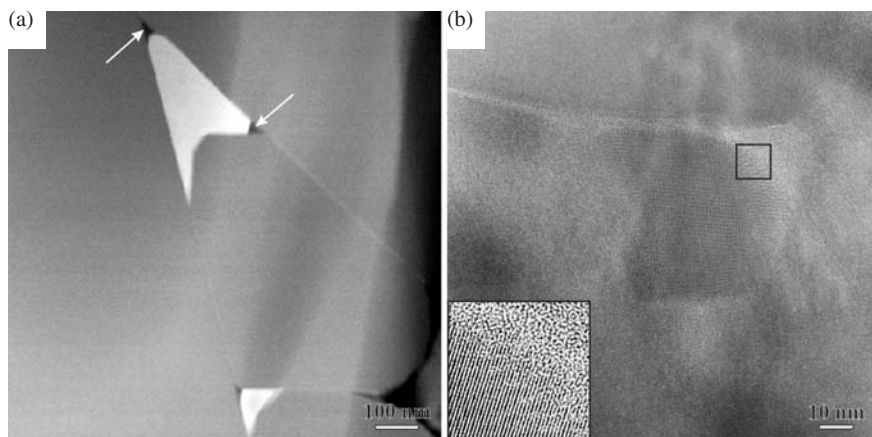

Fig. 6. (a) HAADF-STEM image of the well-defined homogeneous Y–Al–Si phase occupying the majority of the triple-point pocket region. Small quantities of SiO_2-rich phases observed at the triple junctions are marked by arrows. (b) HRTEM image of a small crystallite and the amorphous phase filling the triple-point pocket between exaggeratedly grown alumina grains. The inset image is from the region marked by the square.
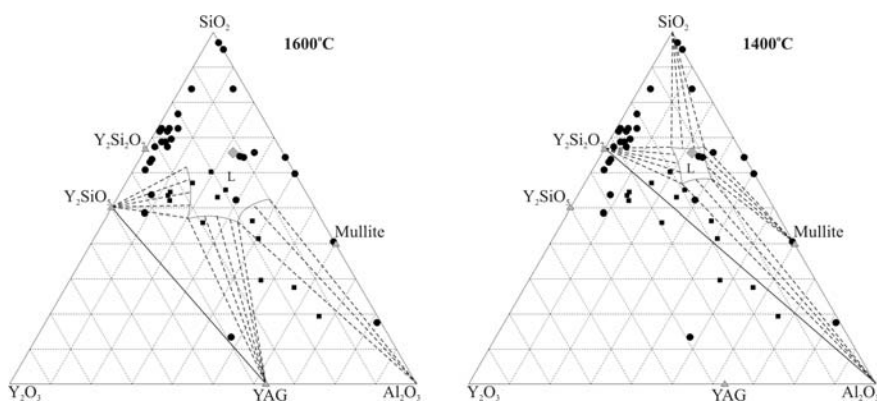
Fig. 7. Experimental points obtained from analysis of TP-pocket phases are presented in the Y_2O_3–Al_2O–SiO_2 ternary system, combined with the reported isothermal section of the Y_2O_3–Al_2O–SiO_2 system at 1400 °C and 1600 °C [19]. Measurements with the overestimated Al_2O_3 concentration are shown as squares (■), whereas measurements that represent the absolute composition of the pocket phases are marked by circles (●). The grey diamond symbol (◆) represents the composition of the lowest ternary eutectic temperature at 1371 ± 5 °C.

lyses. The particles contained only Al, Y and O atoms. In all cases the composition and the electronic structure of the investigated precipitates corresponded perfectly to the YAG phase (Fig. 3b).

4. Discussion

Alumina is one of the most unforgiving hosts for most impurities. The strong segregation of various cations to the internal interfaces of the ceramics has been reported in the past. As a natural consequence of this strong segregation behaviour, most of the properties of the ceramics are strongly influenced by these impurities. The results presented in this study firstly reveal the intricate interplay of two such impurities, i.e., between yttrium and silicon, in the ceramic. Secondly, they show that the chemistries of the interfaces and/or triple-point pockets may also be interpreted using the information provided in the equilibrium phase diagrams for bulk ceramics. However, one has to pay attention to the additional constraints imposed as one considers the chemistries of the confined regions. Several attempts to incorporate terms that will help one understand the behaviour within confined regions of internal interfaces have been reported in the past [29, 30].

This study illustrated additionally that the Si impurity in yttrium-doped alumina could also have a significant impact on the formation sequence of Y–Al–O precipitates that was recently reported [8]. As a natural consequence of such an influence, Si impurities can significantly modify the level of yttrium segregation to the grain boundaries in this system. The following observations in yttrium-doped polycrystalline alumina were made as a function of the Si-contamination concentration:

1. No Si impurities – Clean, Y_2O_3-doped alumina samples could be sintered close to full density with normal grain-growth behaviour. The Y atoms segregated to the grain-boundary core. The precipitation in this sample started with the formation of the structurally simple YAP phase instead of the equilibrium YAG phase.

2. The Si-contaminated Y_2O_3-doped alumina samples showed a bimodal grain-size distribution of the considerably larger alumina grains and the fine-grained alumina matrix. In the presence of the Si impurity the precipitation resulted in the formation of the structurally complex YAG phase. These samples revealed triple-point pockets full of Y–Al–Si–O glass and Y–Si–Al–O crystalline phases.

The discrepancy between the precipitation behaviours observed in this study of clean, yttrium-doped alumina samples and the samples reported in the literature may be explained by the presence of some undetected, additional impurities. Small amounts of certain impurity atoms could, in combination with Y, drastically improve the diffusivity along the grain boundaries [12, 13]. The ease of ionic transport along the grain boundaries may promote the formation of the more complex YAG phase, which requires a larger number of atoms to organize themselves in a crystalline structure. In fact, in many reported studies Si was often detected as the main impurity in the yttrium-doped alumina system [1, 2, 4, 11, 12]. Moreover, the results obtained in this study with *Si-contaminated* yttrium-doped alumina samples support this argument, since all of the observed Y–Al–O precipitates in the Si-contaminated samples were the YAG phase.

It is interesting to note that despite the observed precipitates reported by two different research groups being the YAG phase [3, 5–7], the absolute values of the excess-Y concentration at the grain boundaries differed significantly for these reported studies. Assuming that the possible systematic errors in the measurements were minimized, this discrepancy may be related to the formation of different types of Y–Al–O precipitates in these samples as the precipitate's composition determines the excess-Y concentration at the grain boundaries [8]. Thus, samples with only YAG precipitates are expected to have a lower grain-boundary excess-Y concentration compared to the system with predominately YAP precipitates. In fact, Gülgün and co-workers in their early studies on the same yttrium-doped alumina system as in Ref. [6], rich with Y–Al–O precipitates, reported Γ_Y values of 3.3 ± 0.9 at nm^{-2} [1]. Detailed measurements performed at the grain boundaries of these specimens uncovered the presence of Si impurities. Moreover, these Γ_Y values are close to the values obtained in the studies of Wang et al [6]. In contrast to this, cleaner samples investigated by Gülgün et al. [5] showed significantly higher values of the Y-excess concentration, fixed at around 6 at nm^{-2}. They claimed that to the best of their knowledge these sets of samples were purer than any of those previously reported in the literature, with the amount of Si generally below the detection limits of the available experimental techniques (<0.3 Si-atoms nm^{-2}). In fact, the values of Γ_Y obtained in our study of yttrium-doped alumina with YAP precipitates were 5.5 at nm^{-2}, which is reasonably close to the latter values.

The coinciding observations of the promotion of AGG and the formation of YAG precipitates instead of the much

^AApplied

S. Šturm et al.: The role of Si impurities in the transient dopant segregation and precipitation in yttrium-doped alumina

simpler YAP phase when Si and Y impurities are coexisting is interpreted in terms of the Si and the Y at the alumina grain boundaries being the cause of a structural transformation of the grain-boundary core, as reported by MacLaren et al. [12]. According to our studies the critical Γ_Y and Γ_{Si} values for such a grain-boundary transformation are between $4-5$ at nm^{-2}. As a consequence, first it is possible to precipitate a Y–Al–O phase that has a large and complicated unit cell instead of the simpler YAP phase. At the same time, facilitated kinetics in the alumina grain boundaries, which are otherwise rather slow, allows the boundaries to move at high rates by a solution–re-precipitation process.

The dynamics and chemistry of the grain boundaries could be best studied at high temperatures. The analyses performed at room temperature revealed that the liquid phase in the triple-point pockets in this system underwent a phase separation during cooling. A liquid-phase separation was predicted for the equilibrium Y_2O_3–Al_2O_3–SiO_2 ternary system [19, 20]. Phase separation was illustrated by HAADF-STEM and HRTEM observations that exposed the crystallites located inside triple-point pockets, while the corners of the triple-point pockets were filled with an amorphous phase (see Fig. 6). This shows that the boundaries had a thin, liquid film at high temperatures, which crystallized during the cooling stage. The Si–Y-rich lens-like precipitate entrapped between two large grains is explained by the formation from the liquid grain-boundary film/phase during the cooling period (see Fig. 6).

When all the measured compositions of the triple-point pockets and crystalline phases contained within are plotted on the equilibrium ternary phase of the system, a map for the cooling path of the system emerges. As expected, the phase separation happened towards equilibrium concentrations of the crystalline phases in the system. The amorphous regions left surrounding the crystalline phases appear to be close to the last remaining liquid composition in the lowest eutectic. The deviations from the exact compositions predicted by the equilibrium phase diagram could possibly be explained by the additional thermodynamic constraints imposed by the confinement of the surrounding surfaces and the kinetics of cooling. At this stage, instead of trying to give definite explanations for the compositions measured, they are merely marked on the phase diagram to facilitate further discussions and studies.

5. Conclusions

From this study it was confirmed that clean, yttrium-doped alumina can be successfully sintered to densities in excess of 99 % of the theoretical density without experiencing any abnormal grain growth. The Y grain-boundary coverage was fairly homogeneous, with a mean value of $\overline{\Gamma}_Y = 5.5$ at nm^{-2}. No impurities other than Y were detected in this specimen, within the detection limits of the analytical technique used. The Y–Al–O precipitates observed in the clean, Y_2O_3-doped alumina specimen were YAP. In contrast, only the YAG phase was present in the SiO_2-contaminated Y_2O_3-doped alumina samples. The critical amount of Y and Si at the grain boundaries in these samples to promote the structural transformation of the grain-boundary core was determined to be between $4-5$ at nm^{-2}. Such a transformation could accelerate the dif-

fusivity along and across the grain boundary, which resulted in both lower kinetic constraints in the formation of the YAG second phases and at the same time allowing grain boundaries to move at high rates by a solution–re-precipitation process, thus inducing AGG. According to the SiO_2–Y_2O_3–Al_2O_3 equilibrium ternary phase diagram the compositions of the TP-pocket phases found in the region of the exaggeratedly grown alumina grains indicate the presence of alumino-silicate bulk liquids at the sintering temperature.

References

[1] M.A. Gülgün, V. Putlayev, M. Rühle: J. Am. Ceram. Soc. 82 (1999) 1849. DOI:10.1111/j.1151-2916.1999.tb02008.x
[2] M.A. Gülgün, M. Rühle, in: T. Sakuma, K. Yagi (Eds.), Key Engineering Materials, 171–174, Transtec Publications, Zürich-Uetikon, Switzerland (1999) 793.
[3] R. Voytovych, I. MacLaren, M.A. Gülgün, R.M. Cannon, M. Rühle: Acta Mater. 50 (2002) 3453. DOI:10.1016/S1359-6454(02)00159-3
[4] P. Gruffel, C. Carry: J. Am. Ceran. Soc. 11 (1993) 189. DOI:10.1016/0955-2219(93)90087-8
[5] M.A. Gülgün, R. Voytovych, I. MacLaren, M. Rühle, R.M. Cannon: Interface Sci. 10 (2002) 99. DOI:10.1023/A:1015268232315
[6] C.M. Wang, G.S. Cargill III, H.M. Chan, M.P. Harmer: Acta Mater. 48 (2000) 2579. DOI:10.1016/S1359-6454(00)00076-8
[7] C.M. Wang, G.S. Cargill III, H.M. Chan, M.P. Harmer: Interface Sci. 8 (2000) 243. DOI:10.1023/A:1008717820000
[8] M.A. Gülgün, S. Šturm, R.M. Cannon, M. Rühle: Int. J. Mater. Res. 99 (2008) 1324.
[9] J.S. Abell, I.R. Harris, B. Cockayne, B. Lent: J. Mater. Sci. 9 (1974) 527. DOI:10.1007/BF02387524
[10] G.T. Adylov, G.B. Voronov, E.P. Mansurova, L.M. Sigalov, E.M. Urazaeva: Russ. J. Inorg. Chem. (English Translation) 33 (1988) 1062.
[11] D. Bouchet, F. Dupau, S. Lartigue-Korinek: Microsc. Microanal. Microstruct. 4 (1993) 561. DOI:10.1051/mmm:0199300406056100
[12] I. MacLaren, R.M. Cannon, M.A. Gülgün, R. Voytovych, N. Popescu-Pogrion, C. Scheu, U. Täffner, M. Rühle: J. Am. Ceram. Soc. 86 (2003) 650. DOI:10.1111/j.1151-2916.2003.tb03354.x
[13] S.J. Dillon, M.P. Harmer: Acta. Mater. 55 (2007) 5247. DOI:10.1016/j.actamat.2007.04.051
[14] S.J. Dillon, M. Tang, W.C. Carter, M.P. Harmer: Acta Mat. 55 (2007) 6208. DOI:10.1016/j.actamat.2007.07.029
[15] J.D. Powers, A.M. Glaser: Interface Sci. 6 (1998) 23. DOI:10.1023/A:1008656302007
[16] D. Kolar: Ceramic Transactions 7 (1988) 529.
[17] H.-G. Bang, J.-H. Song, S.-Y. Park: Mater. Sci. Forum 510–511 (2006) 474. DOI:10.4028/www.scientific.net/MSF.510-511.474
[18] C. Greskovich, J. Brewer: J. Am. Ceram. Soc. 90 (2007) 1375. DOI:10.1111/j.1551-2916.2007.01543.x
[19] U. Kolitsch, H.J. Seifert, T. Ludwig, F. Aldinger: J. Mater. Res. 14 (1999) 447. DOI:10.1557/JMR.1999.0064
[20] O. Fabrichnaya, H.J. Seifert, R. Weiland, T. Ludwig, F. Aldinger, A. Navrotsky: Z. Metallkd. 92 (2001) 1083.
[21] J.H. Yoo, J.C. Nam, S. Baik: J. Am. Ceram. Soc. 82 (1999) 2233.
[22] F.J.T. Lin, L.C. De Jonghe: J. Am. Ceram. Soc. 80 (1997) 2269.
[23] J.A.S. Ikeda, Y.-M. Chiang, A.J. Garratt-Reed, J.B. Vander Sande: J. Am. Ceram. Soc. 76 (1993) 2447. DOI:10.1111/j.1151-2916.1993.tb03965.x
[24] U. Alber, H. Müllejans, M. Rühle: Ultramicroscopy 69 (1997) 105. DOI:10.1016/S0304-3991(97)00036-3

A Applied

S. Šturm et al.: The role of Si impurities in the transient dopant segregation and precipitation in yttrium-doped alumina

[25] T. Gemming, S. Nufer, W. Kurtz, M. Rühle: J. Am. Ceram. Soc. 86 (2003) 581. DOI:10.1111/j.1151-2916.2003.tb03344.x
[26] Z. Horita, T. Sano, M. Nemoto: J. Microsc. 143 (1986) 215.
[27] J.D. Cawley, J.W. Halloran: J. Am. Ceram. Soc. 69 (1986) C 195.
[28] A.M. Thompson, K.K. Soni, H.M. Chan, M.P. Harmer, D.B. Williams, J.M. Chabala, R. Levi-Setti: J. Am. Ceram. Soc. 80 (1997) 373.
[29] C.M. Bishop, R.M. Cannon, W.C. Carter: Acta Mater. 53 (2005) 4755. DOI:10.1016/j.actamat.2005.07.008
[30] C.M. Bishop, M. Tang, R.M. Cannon W.C. Carter: Mater. Sci. Eng. A 422 (2006) 102.

Bibliography

Correspondence address

Dr. Sašo Šturm
Jožef Stefan Institute, Department for Nanostructured Materials
Jamova cesta 39, SI-1000 Ljubljana, Slovenia
Tel.: +386 1 477 3418
Fax: +386 1 477 3221
E-mail: saso.sturm@ijs.si

You will find the article and additional material by entering the document number **MK110258** on our website at *www.ijmr.de*